Weather and Climate Extremes 36 (2022) 100459

Contents lists available at ScienceDirect

Weather and Climate Extremes

journal homepage: www.elsevier.com/locate/wace

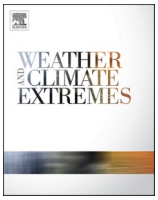

Climate projections at a convection-permitting scale of extreme temperature indices for an archipelago with a complex microclimate structure☆

Juan C. Pérez *, Francisco J. Expósito, Albano González, Juan P. Díaz

Grupo de Observación de la Tierra y la Atmósfera (GOTA), Universidad de La Laguna (ULL), Canary Islands, Spain

ARTICLE INFO

Keywords:
Extreme temperatures
Archipelago
Future projections
Complex orography
WRF
Return temperatures

ABSTRACT

In island systems with complex orography (e.g. Canary Islands), obtaining projections of climate extremes throughout the 21st century is necessary to evaluate the possible adverse effects of climate change. In this work, a dynamic downscaling methodology was applied to obtain the projections of temperature extremes indices. The WRF modeling system was properly configured with a spatial resolution of 3 km, for the periods: 2030–2059 (MID) and 2070–2099 (END), and for the RCPs 4.5 and 8.5 scenarios. This spatial-temporal resolution allows better modeling of the land-surface coupling processes (e.g., latent and sensible heat fluxes), which are one of the main sources of uncertainties in temperature extremes modeling. The initial and boundary conditions were defined by three CMIP5 Earth Systems Models: GFDL-ESM2M, MIROC-ESM, and IPSL-CM5. The future changes were calculated against the modeled reference period was 1980–2009 (HIS). The selected extremes indices were those defined by the Team of Experts on Climate Change Detection and Indices (ETCCDI) and were: monthly absolute maximum and minimum temperature respectively (TX and TN), monthly maximum of the diurnal temperature range (DTR), tropical nights (TR), warm days (TX90P), cold nights (TN10P), warm-spell duration index (WSDI) and cold-spell duration index (CSDI). Also, the return levels and return periods for annual maximum temperature were analyzed using the Generalized Extreme Value distribution (GEV).

The modeled indices were compared with those obtained from observations at nine ground-based stations for the HIS period. Despite the high spatial and temporal resolution of the models a bias is still observed between the modeled and observational values for the absolute indices, even when the simulations are driven by reanalysis data. However, the comparison of these indices around their previously unbiased means yields values on average of 0.85 with a standard deviation of 0.06 on a Perkins-based skill score. Regarding the 20-year return levels for maximum temperature, differences between the average of the models and observations are below 2 °C for all sites, except for the highest stations IZO and TFN, which reach 2.9 and 4.2 °C, respectively.

The analyses of the results indicate that the future projections of the indices obtained using any of the models remain constant from the mid-century to the end of the century for the RCP45 whereas they continue to increase if the RCP85 is considered. This finding shows that all models closely follow the variation in the CO_2-equivalent concentrations used as input. Thus, TX and TN are expected to increase, with an average change for the END period and RCP8.5 of 4.0 ± 0.5 °C and 4.4 ± 0.4 °C for TN. TX90p increases considerably (30 percentage points), and the TN10p index will be close to zero. The increase in temperatures is mainly due to, in addition to the modification of the synoptic patterns, a decrease in total cloud cover and soil moisture.

This decrease in soil moisture has a direct effect on the decrease in latent heat flux and an increase in sensible heat flux, associated with a projected increase of DTR. Also, the 20-year return levels for maximum temperature obtained for the HIS period will correspond to return periods between 1 and 6 years at the END period and RCP8.5.

☆ These authors contributed equally to this work.

* Corresponding author.
E-mail address: jcperez@ull.edu.es (J.C. Pérez).

https://doi.org/10.1016/j.wace.2022.100459
Received 6 October 2021; Received in revised form 17 March 2022; Accepted 25 April 2022
Available online 28 April 2022

1. Introduction

The study of the evolution of the extreme values of temperature distribution in a climate change scenario is crucial due to its influence on such important societal and economic aspects as human health, energy demand, ecosystem conservation, agriculture, water resources, etc. Among the conclusions of the IPCC Fifth Assessment Report, Hartmann et al., 2013 pointed out that changes in extreme weather and climate events have been observed since about 1950. Regarding the temperature extremes, they add that it is very likely that the number of cold days and nights has decreased and the number of warm days and nights has increased on a global scale during the last decades. Also, an increase in the frequency of heatwaves in large parts of Europe, Asia, and Australia is very likely (Hartmann et al., 2013). Accurate modeling of these extreme observations is a priority to establish a solid foundation for obtaining reliable climate projections throughout this century. Various studies show that the Coupled Model Intercomparison Project (CMIP) 5 and CMIP6 models tend to overestimate the hot day extremes and underestimate cold night extremes, either on a global or regional scale (Di Luca et al., 2020a; Sillmann et al., 2013). An analysis of the possible error sources has demonstrated that the overall performance of CMIP ensembles improves when increasing the horizontal resolution mainly because of the better representation of the synoptic-scale variability (Di Luca et al., 2020b).

Several studies focused on reducing uncertainties in temperature modeling concluded that those land-surface coupling processes, which are difficult to simulate, play an important role (Stegehuis et al., 2013). These authors show that the model ensemble spread (as a measure of uncertainty) of temperature is reduced using observational-based heat flux data. Whan et al. (2015), find an important impact of soil moisture (and thus heat flux) on extreme maximum temperatures in Europe. Freychet et al. (2021), state that the observed difference between extreme temperature modeling data is related to differences in land-atmosphere feedback between models. Using an emergent constraint (ΔTX and TX98p), applied to the CMIP5 and CMIP6 models and the ERA5 reanalysis, based on surface heat fluxes (latent and sensible) as an indicator of land-atmosphere interaction, they found a relationship between surface moisture (land-surface process) and TX variability and uncertainties in projection of TX98p.

The islands are among the most sensitive regions in the world regarding the potential adverse effects of climate change along the 21st century (Nurse et al., 2014). The main climate-related drivers of risk for islands include: sea-level rise, tropical and extratropical cyclones, increasing air and sea surface temperature, and changing rainfall patterns. Also, small and orographically complex islands are, in general, natural ecosystems extraordinarily rich in endemism, contributing greatly to the global biodiversity (IPBES, 2019; Kier et al., 2009), and usually have fragile socioeconomic structures, which are very dependent on climate factors (tourism, coastal infrastructures, energy and food dependencies, hydric resources, transportation logistics, etc.).

Varotsos et al. (2021) used dynamical downscaling (a sub-ensemble of five RCMs from the EURO-CORDEX modeling experiment with a horizontal resolution of 0.11°) to obtain climatic projections over the Mediterranean islands of Sicily, Crete, and Cyprus. They found a robust increase for both the mean maximum and minimum temperatures, as well as for the temperature-related extremes under RCP4.5 and 8.5. For the Pacific islands an increase of +2.0–4.0 °C at the end of the century in the 20-year return temperatures was projected (ABM and CSIRO, 2014).

One of the zones where the natural ecosystems are of outstanding biological, hydrological, and socioeconomic value is the Macaronesian region (Azores, Madeira, Canary Islands and Cape Verde) (Sperling et al., 2004). As an example, the main industry in the Canaries is tourism (based on their climatic conditions), being these islands one of the most important tourist destinations in the European Union where 40% of employment and 35% of gross domestic product (GDP) depend on this sector. The Canary Islands have a population of 2.2 million people, receiving an influx of more than 13.0 million foreign tourists per year (ISTAC, 2021). Thus, the study of possible future changes of the climatic conditions, and particularly in extreme temperatures, is extremely important in this region.

Several studies have addressed the realization of climate projections in the Canaries both with dynamical downscaling (Pérez et al., 2014; Expósito et al., 2015) and with statistical approaches (AEMET, 2021). Also, the possible changes along this century of renewable resources were studied (González et al., 2017; Pérez et al., 2019). All of these works that used dynamical downscaling are based on the pseudo global warming (PGW) methodology with a resolution of 5 km. However, the main drawback of the PGW methodology is its limitation for some studies related to extreme values, since PGW does not consider all possible mechanisms producing climate changes. For example, they miss some non-linear changes in dynamics.

On the other hand, the Canaries, and the Macaronesian region in general, are islands with complex orography. For example, on the island of Tenerife, there are vertical differences of more than 3 700 m (Teide peak) in less than 15 km horizontally, or 2 200 m in less than 10 km in La Palma. This orography jointly with the climatic predominant conditions (mainly, the trade winds and the thermal inversion layer) configure an intricate set of microclimates, which can be observed in the Climate Atlas of the archipelagos of the Canary Islands, Madeira, and the Azores (Climate Atlas, 2012). Pérez et al., (2014), showed that performing simulations at convection-permitting scales adequately reproduce the land-atmosphere-sea interaction processes (surface wind, convection, cloud formation, …). As indicated by these previous studies these processes are at the center of changes that can affect the evolution of extreme temperatures, such as a possible change in the dominant cloud regime (marine stratocumulus) to shallow cumulus clouds (Díaz et al., 2019), or a decrease in cloud cover in winter (Pérez et al., 2019) and a decrease in surface winds in summer (González et al., 2017).

Considering this climatic scenario on archipelagos together with the fact that the bibliography on these topics is scarce and mainly focused on sovereign state small islands (Petzold and Magnan, 2019), the goal of this work is to obtain reliable projections of climatic extreme temperatures for the Canary Islands using an appropriate downscaling approach with an adequate (high) resolution. This study will be useful for the design of effective adaptation/mitigation strategies in this archipelago.

In the next point, the observational data and the temperature extreme indices are described. In section 3, the modeling strategy (dynamical downscaling) is shown and the possible uncertainties are discussed. The climate projections of extreme indices, with a resolution of 3 km, throughout this century, using 3 CMIP5 models as the initial and lateral boundary conditions for the Representative Concentration Pathways (RCP) scenarios 4.5 and 8.5 are shown in the fourth one. The conclusions are outlined in the fifth point.

2. Observational data set and temperature extremes indices

The observational information used in this study was obtained from the European Climate Assessment and Dataset (ECAD, 2021; Klok and Tank, 2009; Klein et al., 2002). ECAD gathers data from 65 countries throughout Europe and the Mediterranean from a total of 20, 168 meteorological stations. In this type of long-term time series, obtained from different sources, the homogeneity assessment is a crucial aspect in the quality control of the data. In this database, the Wijngaard et al. (2003) methodology was implemented to test the daily surface air temperature and precipitation. Using the daily maximum and minimum temperature (Tx and Tn, respectively), ECAD produces the extreme indices defined by the Team of Experts on Climate Change Detection and Indices (ETCCDI) (Klein Tank et al., 2009; Zhang et al., 2011). ECAD provides two types of indices: absolute indices obtained directly from the extreme values, and threshold variables, which require a threshold level computed from a reference period. As ECAD uses the reference period 1961–1990, the indices were recalculated using HIS as the

reference period to match the model experiments. To this aim Climate Data Operator (CDO) software was used, which is a collection of tools implemented specifically for the standard processing of climate and forecast model data (Schulzweida, 2019). The extreme temperature indices analyzed in this work are described in Table 1.

The observational absolute and threshold indices were analyzed in nine ground-based stations over the Canary Islands (Table 2), which were also used to estimate the uncertainties in these magnitudes obtained through modeling. Most of these sites are located at the airports of each island with altitudes close to sea level. However, the IZO and TFN stations are located at 2 731 and 632 masl, respectively.

3. Modeling methodology

3.1. Model setup

To obtain a better representation of the processes that affect climate extremes in a region such as the Canary Islands, increasing the horizontal resolution of the simulations is necessary. With this objective, a dynamic downscaling technique was used based on the Weather Research and Forecast (WRF) model (Skamarock et al., 2008). The WRF version (3.4.1), the configuration and the vertical levels of the simulations were selected following the results of a previous sensitivity study also focused on this archipelago (Pérez et al., 2014). Three domains were defined with resolutions of 27, 9 and 3 km in a one-way nesting configuration (Fig. 1), and all of them with 32 vertical eta levels. The results analyzed in this work were those obtained in the innermost domain (3 km), for the periods: 1980–2009, 2030–2059, and 2070–2099, and for two greenhouse gas emission scenarios throughout the 21st century: RCP4.5 and RCP8.5 (Taylor et al., 2012). All the simulations for each of these three time periods were initialized one year before to provide an initial spin-up period for the model physics. The data from this first year were excluded from any subsequent data analysis. The cloud microphysical processes were parameterized using the WRF double moment 6-class (WDM6) scheme (Lim and Hong, 2010). The radiation scheme was set to the Community Atmosphere Model with gas concentrations adjusted to each scenario (Collins et al., 2004). The land surface model was established according to the Noah model (Chen and Dudhia, 2001) and the planetary boundary layer scheme was characterized using the Yonsei University scheme (Hong et al., 2006). Additionally, the cumulus parameterization scheme of Kain-Fritsch (Kain and Fritsch, 1990) was only used in the 2 outermost domains (D1 and D2). In the innermost domain (D3) no cumulus parameterization was applied because at these resolutions the fluxes are explicitly resolved (Skamarock et al., 2019). This WRF configuration was selected by Pérez et al. (2014) as that having the minimum errors between a set of different configurations tested in the Canaries region.

The climate simulations were driven by global circulation models (GCM) included in the CMIP5 project which provided the initial and lateral boundary conditions. The choice of the models used as boundary conditions for the regional simulations is a key aspect in the design of any climate regionalization experiment. In this work, three GCMs were selected based on previous studies for the African CORDEX domain (Ito et al., 2020) and the availability of the necessary data with adequate temporal resolution: GFDL-ESM2M (Dunne et al., 2013), MIROC-ESM (Watanabe et al., 2011) and IPSL-CM5A-MR (Dufresne et al., 2013), using the realization r1i1p1 for all of them.

Table 1
Definition and units of the indices used.

Absolute indices:		
Acron.	Name and definition	Units
TX	Monthly maximum; the monthly maximum of daily maximum temperature (Tx).	°C
TN	Monthly minimum; the monthly minimum of daily minimum temperature (Tn).	°C
DTR	Monthly maximum diurnal temperature range; the monthly maximum of the daily diurnal temperature range.	°C
Threshold indices:		
Acron.	Name and definition	Units
TR	Annual tropical nights; the number of days in a year with Tn > 20 °C	days per year
WSDI	Warm-spell duration index; the annual count of days with at least 6 consecutive days with Tx > 90th percentile of daily maximum temperature for a given calendar day. The 90th percentile is calculated for a 5-day window centered in the given calendar day.	days per year
WSDIn	Warm-spell duration index events; the annual count of events with at least 6 consecutive days with Tx > 90th percentile.	# events per year
CSDI	Cold-spell duration index; the annual count of days with at least 6 consecutive days with Tn < 10th percentile of daily minimum temperature for a given calendar day. The 10th percentile is calculated for a 5-day window centered in the given calendar day.	days per year
CSDIn	Cold-spell duration index events; the annual count of events with at least 6 consecutive days with Tn < 10th percentile.	# events per year
TX90p	Warm days; the number of days in a month with Tx > 90th percentile, calculated for a 5-day window centered in the given calendar day.	days per month
TN10p	Cold nights; the number of days in a month with Tn < 10th percentile, calculated for a 5-day window centered in the given calendar day.	days per month

3.2. Model evaluation

To evaluate the uncertainties introduced by the WRF model, the outputs of the simulation-driven by ERA-Interim reanalysis for the period 1995 to 2004 (Pérez et al., 2014) were compared to the ECAD observational data. The WRF settings selected in the present study are the same as those implemented in that work, including the WRF version and the number of vertical levels. The main difference was the spatial resolution, since in the work of Pérez et al. (2014) it was performed at 5 km instead of the 3 km used in this one.

Fig. 2 shows the Q-Q plots of the simulated values corresponding to the closest land grid point to the ECAD stations for the extreme variables TX and TN. Except for the IZO station, the regression of the percentiles has, on average, a slope of 1.20 and 0.95 for TX and TN respectively (ideal = 1.00), with a Pearson correlation coefficient over 0.98. These results show that the model is able to reproduce the dispersion of observational data around the mean. However, this comparison also shows that the model introduces a bias, whose value is, on average, of −2.6 °C and −2.1 °C for TX and TN respectively (IZO removed). Although the grid point used is the nearest to the ECAD stations and they correspond to a land pixel for WRF, some of them, especially those of airports, are influenced by their proximity to the sea. Moreover, the sea surface temperature provided by ERA-Interim has a mean negative bias around −0.3 °C with respect to NOAA OI SST v2 (Huang et al., 2021) for those ocean pixels nearest to the ECAD stations.

In supplementary material (Fig.SM.1–6) the seasonal analysis is shown.

In addition, to evaluate the uncertainties of the WRF simulations driven by the three mentioned GCMs (GFDL, IPSL, MIROC, hereinafter), the observations of the ECAD stations were also compared with the simulated values corresponding to the nearest land grid point. Fig. 3 shows the box-and-whisker plots of the extreme variables for observations (colored), the three models (white, from left to right GFDL, IPSL, MIROC), and the ensemble of the models (light-colored). The size of the boxes represents data dispersion between the 25th and 75th percentiles and the horizontal line within the box corresponds to the median. In these figures, the value zero was included and therefore, due to the high number of zeros in the variables TR, WSDI, and CSDI, the median overlaps that minimum value. Furthermore, for the WSDI and CSDI

Table 2
ECAD stations used in this study, their geographical locations and height, and the model WRF nearest land grid point to the stations.

ECAD CODE and Station		Observation sites			WRF simulation grid point		
		Lat. (°N)	Lon. (°E)	Hgt. (m)	Lat. (°N)	Lon. (°E)	Hgt. (m)
1 388 IZO	Izaña	28.309	−16.499	2 371	28.306	−16.490	1873
0 455 TFN	Tenerife North	28.478	−16.329	632	28.468	−16.328	628
2 970 ACE	Lanzarote	28.952	−13.600	14	28.954	−13.601	13
3 940 FUE	Fuerteventura	28.444	−13.863	25	28.441	−13.871	52
3 957 VDE	Hierro	27.819	−17.889	32	27.820	−17.894	355
3 958 SPC	La Palma	28.633	−17.755	33	28.630	−17.759	39
3 959 SCT	S/C Tenerife	28.463	−16.255	35	28.468	−16.247	16
3 960 TFS	Tenerife South	28.048	−16.561	64	28.036	−16.571	5
3 941 LPA	Gran Canaria	27.923	−15.389	24	27.928	−15.383	3

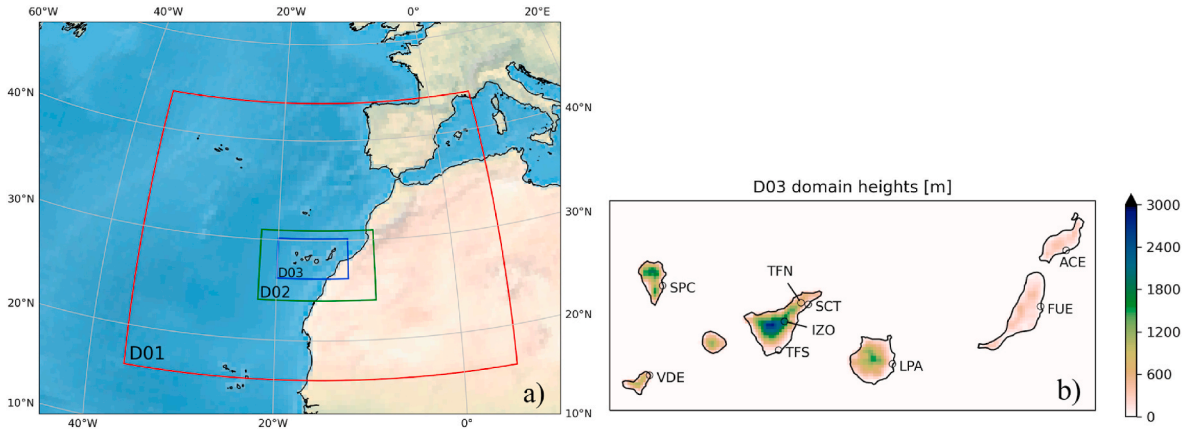

Fig. 1. WRF domains configuration to simulate the extreme data at the Canary Islands, D01 resolved at 27 km, D02 at 9 km and D03 at 3 km (a), and the D03 WRF orography (b).

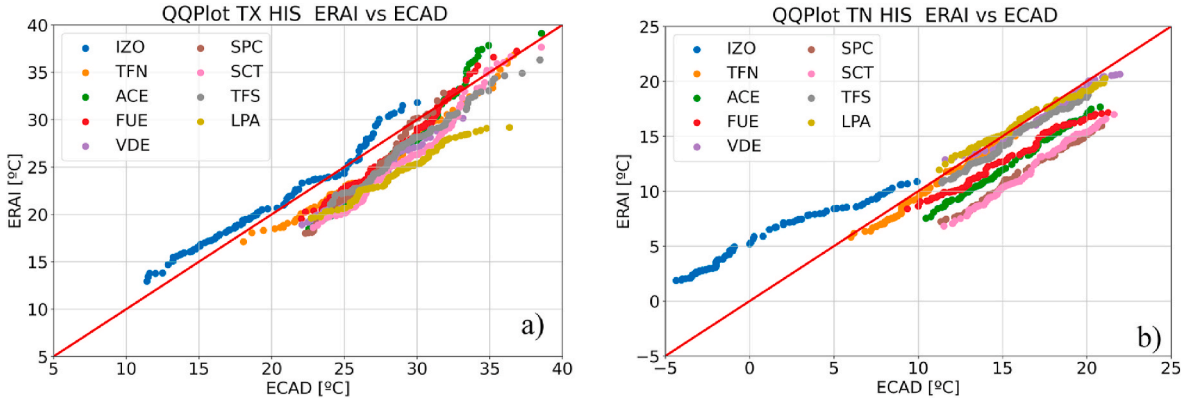

Fig. 2. Q-Q plot of the WRF driven by ERA-Interim reanalysis data for the land grid point closest to the ECAD stations versus the data from these stations for the absolute extreme indices TX (a) and TN (b) in the period 1995–2004. The red line indicates the ideal behavior. (For interpretation of the references to color in this figure legend, the reader is referred to the Web version of this article.)

variables, the minimum number of days required is 6, so observing this value for the median and even for the upper limit of the box plot is possible. This representation shows that, as in the previous case, there is a bias between these datasets. The simulated daily minimum temperatures (Tx and Tn) and therefore the monthly minimum (TX and TN) present an underestimation concerning the ECAD data. The IPSL model generates the lowest values, on average 2.9 and 3.7 °C lower for TX and TN respectively, whereas MIROC produces the closest (0.7 and 1.6 °C lower for TX and TN).

Fig.SM7 – 9 in supplementary materials show the seasonal analysis.

To carry out the comparison between the observational data and the models regarding the dispersion of the values around the mean, the bias observed in the box plots was previously subtracted. First, the distributions were compared using the percentiles in a quantile-quantile plot (Q-Q plot) such that a perfect distribution must fit the line y = x (red diagonal in the figures). This allows identifying the anomalies range for which the model is separated from the observed data. As Fig. 4 shows, the distribution of the temperature anomalies for absolute indices approaches the diagonal that compares the models against ECAD anomalies. However, an increase in the dispersion of the model is observed in the largest deviations and a reduction in the lowest ones for the TX variable. This behavior is common for all three models. The IZO station presents a different pattern than the rest of the stations for TN in all models. It is a very special site located in the central mountain range of

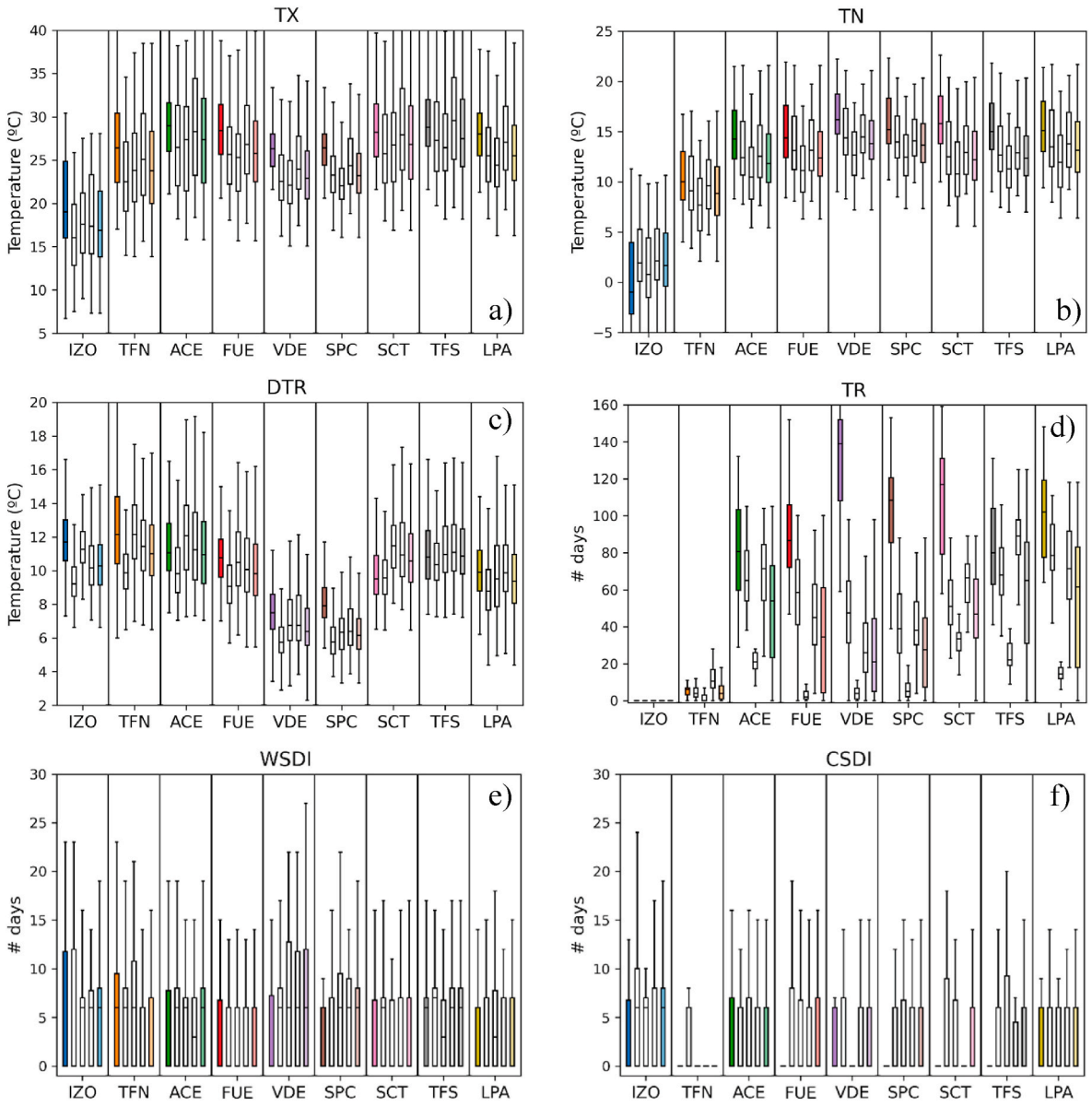

Fig. 3. Box-whisker plots of the ECAD station data (colored), the model GFDL, IPSL, MIROC (white), and ensemble (light color) of the nearest land grid for the TX, TN, DTR, TR, WSDI, and CSDI variables, and for the period 1980–2009 (HIS). The box plot encompasses the 25th and 75th percentiles, whereas the horizontal line within the box corresponds to the median. (For interpretation of the references to color in this figure legend, the reader is referred to the Web version of this article.)

the island of Tenerife, with slopes that change abruptly in very short distances. Probably, due to this situation, the models cannot adequately simulate this area and, therefore, follow the range of extreme temperatures, overestimating the lowest anomalies and underestimating the highest ones (about ±2.5 °C) for this station.

Regarding the threshold variables (Fig. 5), they present a larger dispersion around the diagonal. It is worth highlighting the tropical nights for the IPSL model, in which the observational data show a dispersion that covers 30 days, whereas the modeling is reduced to 20. As mentioned above, the IPSL model produces the lowest TN of the modeled data (second white bar for TN in Fig. 3). Therefore, the monthly minimum temperatures are below the ECAD data, and the number of days in a month in which the threshold of 20 °C is exceeded is lower. For the rest of the simulations, as there is also a reduction in the TN, there exists a decrease in the number of tropical nights and so, for instance, no model has obtained TR for the IZO station, although they appear in the observations. These lower values in TN also result in the observed slopes for the CSDI variable being greater than 1.0 since there are a larger number of consecutive days with lower temperatures than those observed.

In the case of the WSDI, the duration in the number of days for these intervals calculated by the models oscillates around the ideal line for all stations except for the SPC station (La Palma island). This station shows positive ECAD deviations close to 40 days (higher percentiles). Nevertheless, no models reach this accumulative number of consecutive days with continuous high temperatures.

On the other hand, the anomalies were also compared using a second strategy that calculates the Perkins skill score for the probability density functions (PDF) (Perkins et al., 2007). For this procedure, the common area of both distributions was computed using:

$$S_{Score} = \sum_{i=1}^{n} min(P_0, P_S)$$

where P_0 and P_S are the frequency of the observed and simulated anomalies, respectively, in the i-th bin of the total n bins used to obtain

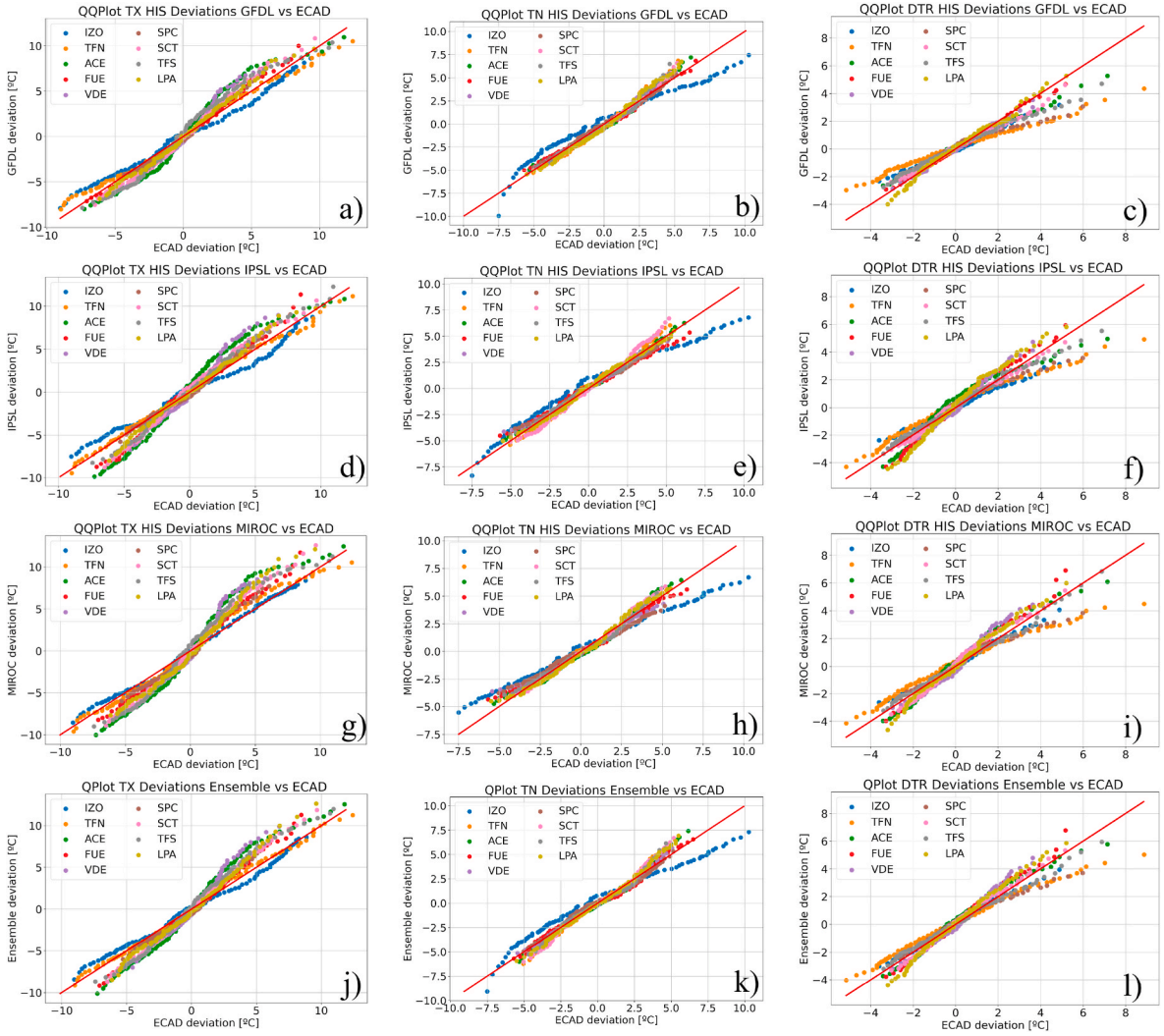

Fig. 4. Q-Q plot of the GFDL, IPSL, MIROC and ensemble models, for the nearest land grid point to the ECAD stations versus the data from these stations for the absolute extreme indices TX (left column), TN (center column) and DTR (right column) in the period 1980–2009 (HIS). The mean was previously subtracted from the data to show the agreement of the dispersion around the mean. The red line indicates the ideal behavior. (For interpretation of the references to color in this figure legend, the reader is referred to the Web version of this article.)

the PDFs. Because the Perkins score depends on the size of the bin, following Ivanov et al. (2018) a 1-unit bin was used in this work (1 °C or one day depending on the index). For this score, under an ideal situation, a value of 1.00 should be obtained.

The skill score for absolute indices and all the stations ranges between 0.68 and 0.96 with a mean of 0.85 ± 0.06, indicating that the probability distribution functions of the anomalies of the absolute variables approach those obtained for the observations (see Table 3). For these parameters, the data indicate that no model is better than the others, obtaining similar values close to the mean. However, concerning the threshold values, the projections made with the MIROC model produce a score that, although it is lower than the anomalies for the absolute variables, exceeds the other models. On average for all stations and models, this value is 0.61 ± 0.26.

3.3. *Return periods and return levels. Generalized extreme values distribution (GEV)*

Another important variable used to evaluate the extreme events in temperature is the return period, T, sometimes called recurrence interval. Assuming a stationary process, which is the main limitation of this method, T is defined as the average time between two consecutive occurrences of a defined event. So, the probability, P, of occurrence of such event in a year is the inverse of the return period (in years). Alternatively, the return level is the value expected to be exceeded on average with probability P (=1/T) in any given year. These two concepts are used in many disciplines to describe risks (Cooley, 2013). The return period and the return level were estimated fitting the generalized extreme value distribution (GEV) to the annual maximum of observational and modeled Tx data. This is an application of the Extreme Value Theorem or the Fisher-Tippett-Gnedenko Theorem. The implementation used in this work is that of the Python package called “pyextreme”. This particular development of the extreme value analysis (EVA) is based on Coles, S., (2001). Between the two main strategies to carry out an EVA, the Block Maxima/Minima (BM) was chosen. BM uses one-year period, so the EVA was applied to the annual (absolute) maximum temperature. The confidence intervals in the return periods were estimated by bootstrapping technique using 1 000 random samples with replacement and a confidence interval of 95% (Mooney and Duval, 1993).

The average values for most of the stations are close to those obtained from the observations, with an overlap in their confidence intervals (Table 4). The results of the MIROC-driven simulation are the closest, with a difference of 0.6 °C on average for all the stations. The confidence interval of the return maximum temperature from the

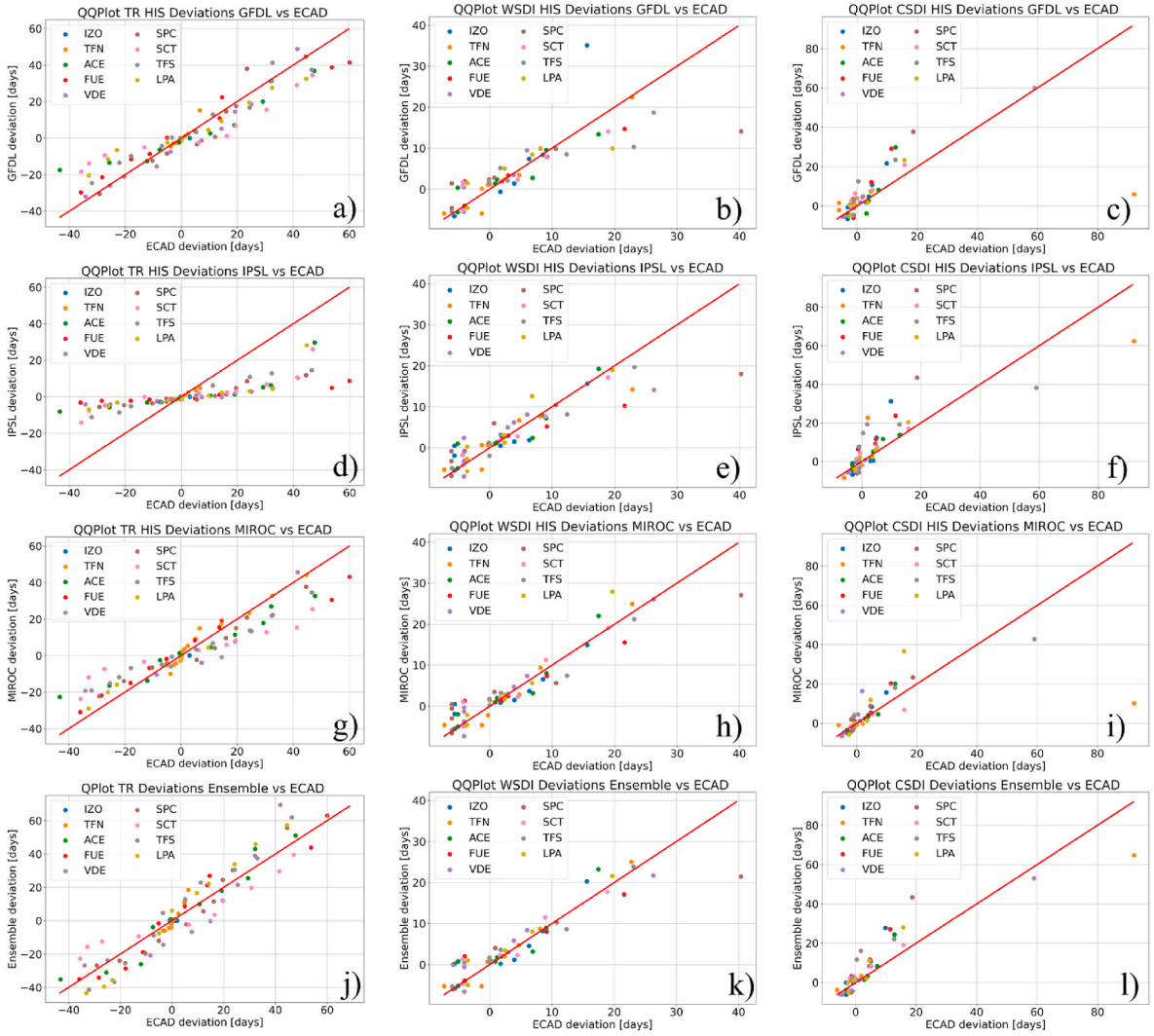

Fig. 5. Q-Q plot of the GFDL, IPSL, MIROC and ensemble models, for the nearest land grid point to the ECAD stations versus the observational data for the absolute extreme indices TR (left column), WSDI (center column) and CSDI (right column) in the period 1980–2009 (HIS). The mean was previously subtracted from the data to show the agreement of the dispersion around the mean. The red line indicates the ideal behavior. (For interpretation of the references to color in this figure legend, the reader is referred to the Web version of this article.)

Table 3
Skill score of the anomalies of the absolute indices (TX, TN, DTR) and the threshold indices (TR, WSDI, CSDI) for the simulations driven by the models GFDL, IPSL, and MIROC, with ECAD as reference (the TR data at the IZO station is zero). The code color indicates the goodness of the skill score (green = 1.00, white = 0.50, and red = 0.00).

VAR	MODEL	IZO	TFN	ACE	FUE	VDE	SPC	SCT	TFS	LPA
TX	GFDL	0.82	0.87	0.76	0.88	0.80	0.91	0.85	0.80	0.89
	IPSL	0.81	0.94	0.68	0.84	0.79	0.88	0.81	0.87	0.90
	MIROC	0.89	0.89	0.69	0.82	0.70	0.82	0.75	0.73	0.78
TN	GFDL	0.73	0.82	0.86	0.88	0.89	0.92	0.89	0.87	0.88
	IPSL	0.79	0.85	0.88	0.86	0.85	0.88	0.86	0.93	0.91
	MIROC	0.75	0.87	0.84	0.85	0.87	0.85	0.88	0.93	0.89
DTR	GFDL	0.83	0.73	0.89	0.92	0.82	0.84	0.89	0.86	0.89
	IPSL	0.84	0.83	0.79	0.83	0.91	0.84	0.86	0.96	0.82
	MIROC	0.92	0.81	0.83	0.87	0.87	0.84	0.83	0.95	0.91
TR	GFDL	*	0.60	0.63	0.70	0.79	0.67	0.43	0.75	0.60
	IPSL	*	0.43	0.37	0.20	0.31	0.37	0.37	0.38	0.30
	MIROC	*	0.63	0.57	0.70	0.67	0.73	0.50	0.65	0.73
WSDI	GFDL	0.87	0.57	0.78	0.82	0.70	0.80	0.68	0.79	0.79
	IPSL	0.63	0.80	0.77	0.90	0.58	0.64	0.77	0.85	0.73
	MIROC	0.73	0.50	0.83	0.77	0.58	0.64	0.8	0.84	0.90
CSDI	GFDL	0.17	0.93	0.84	0.28	0.91	0.77	0.10	0.03	0.10
	IPSL	0.57	0.87	0.77	0.07	0.87	0.24	0.10	0.10	0.83
	MIROC	0.80	0.97	0.87	0.03	0.74	0.09	0.90	0.73	0.83

Table 4
Maximum temperature in degrees Celsius with a 20-year return period obtained in the recent past period, for the observations (ECAD), the three models and their average (Avg.).

	IZO	TFN	ACE	FUE	VDE	SPC	SCT	TFS	LPA
ECAD	29.8 ± 0.8	40.4 ± 1.6	41.5 ± 3.5	37.9 ± 1.1	34.2 ± 1.5	33.0 ± 0.6	39.2 ± 1.0	41.0 ± 2.6	38.8 ± 1.6
GFDL	25.5 ± 0.7	34.2 ± 0.8	38.0 ± 0.4	36.5 ± 1.0	32.4 ± 1.3	31.5 ± 1.0	38.0 ± 1.0	39.5 ± 1.4	36.7 ± 1.4
IPSL	27.2 ± 0.7	36.6 ± 1.1	38.3 ± 0.8	37.2 ± 1.2	32.3 ± 0.8	30.1 ± 0.6	38.1 ± 1.6	39.8 ± 0.8	35.9 ± 1.7
MIROC	27.9 ± 0.7	37.7 ± 1.5	42.5 ± 1.4	40.2 ± 1.5	34.6 ± 0.5	33.4 ± 0.7	41.9 ± 1.3	42.0 ± 0.9	40.7 ± 1.1
Avg.	26.9 ± 0.7	36.2 ± 1.1	39.6 ± 0.9	38.0 ± 1.2	33.1 ± 0.9	31.7 ± 0.8	39.3 ± 1.3	40.4 ± 1.0	37.8 ± 1.4

observations is around 1 °C. These maximum values of temperatures constitute the return levels on which the return periods will be calculated in future projections.

3.4. Current average situation for the extreme temperature indices in the archipelago

Following the usual time frame in Climatology (periods of 30 years), in this work, the reference period was set as the ensemble of the three models (Fig. 6) for the recent past period (HIS, 1980–2009). The mean values and the corresponding 95% confidence intervals were estimated using a bootstrapping strategy generating 1 000 samples with replacement (Efron and Tibshirani, 1994). They are shown in the supplementary material (Fig.SM. 10). These data produce images with a geographic pattern for the extreme variables TX and TN, which reproduce the topography of the terrain. Thus, the highest temperatures are obtained in coastal areas and on islands with less relief. As expected, we observe the maximum values in the southern part of the islands and the eastern ones (Climate Atlas, 2012). Whereas, for the minimum temperature, the lowest values correspond to the highest altitude areas of the archipelago, mainly the center of the islands of La Palma and Tenerife. The trade winds (NE-SW direction) are predominant in this region, bringing cool and humid air, and softening the temperatures in the windward areas. In addition, in the north of the islands of greater relief, an extensive area of stratocumulus is usually formed, so this region is less exposed to solar radiation than the area to the S-SE. As a consequence, the daily range of temperatures is lower in the north than in the south. Moreover, in the SW zone, as it is protected from the trade wind, the minimum daily temperatures exceed the threshold of 20 °C more easily than in the north zone. Thus, that region contains the grid points with the highest number of tropical nights.

The study of the change in the return periods, using the projected data (future time periods), for those return values that in the HIS period are obtained with return periods of 20 years, also provide valuable information on the change in the occurrence of high temperature events.

Fig. 7 shows the average of the three models concerning the 20-year return level for maximum temperature in the recent past. These 20-year return levels will be used in the point 4.2 to study the changes in the return periods throughout the 21st century. Mainly, the southern part of the islands, as well as the eastern islands, are those that show the highest temperatures with values around 40 °C. The western islands and mountain areas provide the lowest values for this parameter.

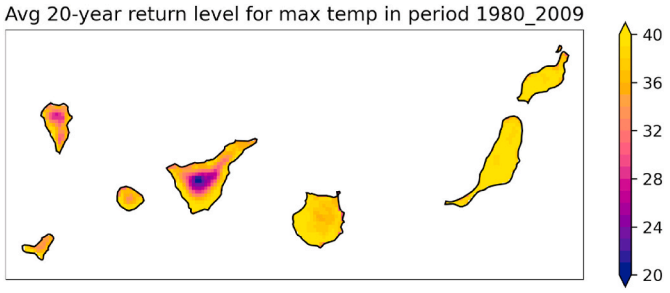

Fig. 7. 20-year return level for the maximum temperature in the period 1980–2009 obtained as the average of the three simulations.

4. Projections along of the 21st century

4.1. Absolute and threshold indices

To observe the changes in the variables studied, the differences between the projections of the ensembles for the future, MID (2030–2059) and END (2070–2099) 21st-century simulation results, and those of the recent past period, HIS (1980–2009) were compared. For future projections, the two greenhouse emission scenarios RCP4.5 and RCP8.5 were considered (Fig. 8). They correspond to an intermediate greenhouse gas emission situation for the future and the worst situation, respectively (van Vuuren et al., 2011).

To evaluate the uncertainties in the projected changes provided by the simulations, a bootstrapping strategy with at least 1 000 samples for each grid point was used. A value of a grid point was considered statistically significant using these differences if its limit of the confidence interval (2·σ) does not include the zero value. This ensures with 95% confidence that the difference between the data is not equal to 0.

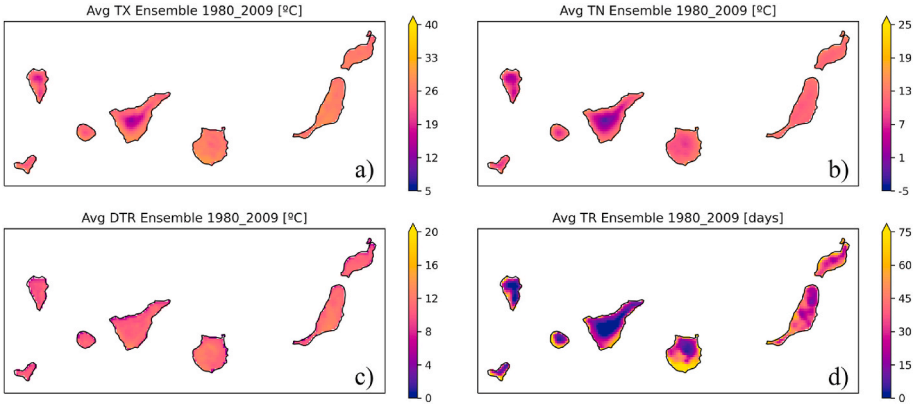

Fig. 6. Ensemble of the three CMIP5 driven simulations for TX (°C), TN (°C), DTR (°C), and TR (days) for the recent past period, 1980–2009 (HIS).

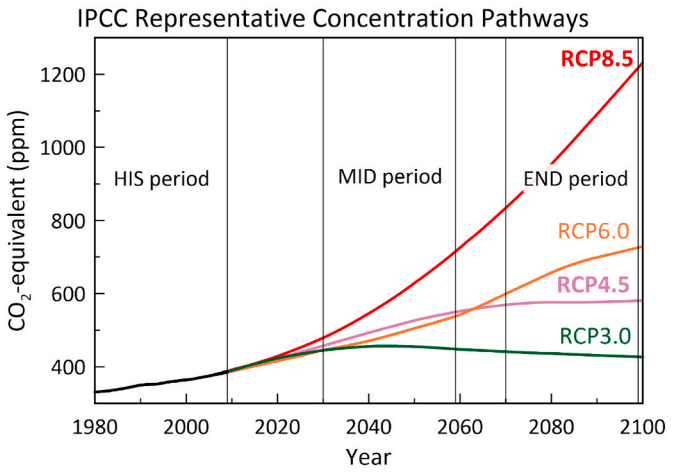

Fig. 8. CO_2-equivalent concentration for the Representative Concentration Pathways of the IPCC. Data from Meinshausen et al. (2011).

The future projections in the MID period show that the differences in TX and TN with regards to the recent past are lower than 0.3 °C between the RCP scenarios. A value of 1.5 ± 0.5 °C is obtained in the average for the increase in TX, whereas a value of 1.4 ± 0.4 °C is found in the case of TN, both for the RCP4.5 scenario. If RCP8.5 is considered the values are 1.2 ± 0.5 °C for TX and 2.4 ± 0.4 °C for TN. However, the behavior changes at the end of the century with an acceleration of the temperature increase in the RCP8.5 scenario compared to RCP4.5. Variations close to 4.0 ± 0.5 °C in TX and 4.4 ± 0.4 °C in TN for END–HIS RCP8.5 are observed, whereas this value in the RCP4.5 is about 2.0 ± 0.5 °C and 2.7 ± 0.4 °C for TX and TN, respectively. This behavior is consistent with the value of the CO_2-equivalent concentration of the RCPs: for the RCP4.5, the amount of this greenhouse gas remains almost constant after the middle of the century, whereas there is a continuous increase in the case of RCP8.5 (Fig. 8) (Meinshausen et al., 2011). Notably, as was previously indicated by Expósito et al. (2015) for the future projections of temperature, the largest extreme increase occurs in the central part of the islands with greater relief. In supplementary material additional results are shown for each of the models separately (Fig.SM.19–22).

These projections indicate that TX and TN increase analogously as they approach the end of the century in any scenario (see Figs. 9 and 10). For this reason, the daily temperature range remains very stable in all projections regardless of the RCP used, never exceeding on average the value of 0.5 °C (Fig.SM.11 in supplementary material). The variations between the maximum and minimum temperature are more notable in the mountainous areas of the islands, with a maximum of 1 °C comparing the end of the century for RCP8.5 and the recent past; this is because the increase in TX for these areas is somewhat greater than for TN. The 95% confidence interval for the changes is shown in supplementary materials (Fig.SM.15–18).

Regarding the threshold indices, the increase detected in TN also produces a large number of tropical nights. Until the middle of the century, the increase runs parallel between the two scenarios, however, notable changes appear at the end of the century depending on the RCP used. In the case of RCP4.5, the number of TR is similar to the MID period, but if we consider RCP8.5, the number of tropical nights increases, on average, three times in the coastal areas and the eastern

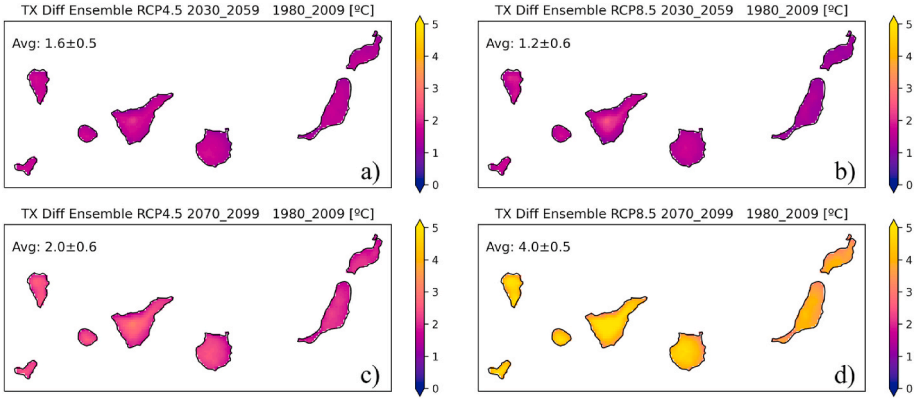

Fig. 9. Average differences for the TX variable (°C) between the simulations for the future projections (MID and END of the century) and the recent past (HIS). They correspond to the greenhouse emission scenarios RCP4.5 (left column) and RCP 8.5 (right column). All the values are statistically significant to a 95% level of confidence.

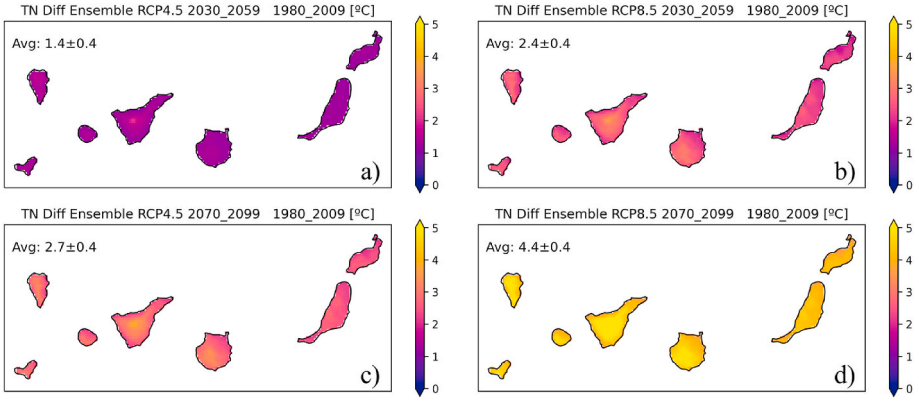

Fig. 10. As Fig. 9 but for the TN variable (°C).

islands (Fig. 11) The study of the future projections of this parameter together with those of maximum temperature is especially interesting given its impact on tourism. The areas with the highest maximum temperatures and tropical nights coincide with the area where most of the hotel infrastructures of the islands are located.

The largest increase observed in the absolute indices at the END period for the RCP85 scenario compared to HIS period is also reflected in the threshold indices. Thus, TX90P increases over 30 percentage points in many areas of the islands in this scenario, but for the RCP45 this value is only observed in the highest areas (Fig. 12). The number of days in a row (more than 6 consecutive) with very high temperatures (WSDI, Fig. 13) as well as the number of events in which this occurs (WSDIn, Fig. SM. 12, supplementary material) also increases in the scenario with the highest radiative forcing at the end of the century. The difference in the number of days exceeds 120 per year in some areas, which indicates that in some months the 90th percentile of the HIS series will be exceeded every day. On the contrary, the TN10P parameter (Fig. 14) is gradually reduced in future projections, reaching values around −10 percentage points for the worst environmental situation, that is, indicating that no point in the image would have minimum temperatures below that obtained for cold nights in the HIS period. Likewise, the values of CSDI and CSDIn (Fig.SM.13-14 supplementary material) also experience reductions, being greater in the western islands than in the eastern ones, with values close to 5 and 3 days respectively.

To find out which are the main causes that give rise to the increase in temperature in future projections, a study of the main variables involved was carried out. To this end, zonal averages of a selected transect in the island of Tenerife were performed (Fig. 15). This island was selected due to its orography, since this allows us to highlight the spatial inhomogeneities, such as the differences between the southern and northern areas, the latter being more exposed to the trade winds, or the effect of the altitude. Although the results are presented for the MIROC-driven simulations similar results were obtained for the other models.

General temperature changes, such as elevation-dependent warming (EDW), are influenced by the prevailing synoptic conditions in the study region. Most of the projections obtained from GCM simulations indicate this enhanced warming of the upper free troposphere, especially in tropical regions, but also evident in subtropical areas (Hartmann et al., 2013). The greater warming at altitudes than near the surface is consistent with wet adiabatic stratification in these areas. Therefore, EDW results in a reduced lapse rate in the future (Bony et al., 2006). The EDW in the Canary Islands was also previously mentioned by Expósito et al. (2015).

Apart from this general influence, there are other mechanisms that affect the local energy balance (Pepin et al., 2015). Some studies in high inland areas point to snow albedo feedback as a crucial aspect of EWD at the local level (Kotlarski et al., 2012; Pepin et al., 2015; Minder et al., 2018). However, because of the short annual period of snow cover on the islands and the small percentage of covered area, it does not play a relevant role in this case. On the other hand, changes in cloud cover, or in cloud properties, affect both shortwave and longwave radiation. In both winter and summer, a future decrease in cloud cover is estimated, especially in the higher areas of the northern slope during winter. In this season, changes in net radiation at the surface level, defined positive downward, are dominated by the shortwave component, with the longwave component remaining very similar to that of the recent past. The increase in solar irradiance largely coincides with a substantial decrease in cloud cover. The effect of this increase of the incident radiation on the temperature response will depend on soil moisture (Pepin et al., 2015). In this particular case, a future decrease in soil moisture is simulated, as a result of a reduction in precipitation, and, consequently, a decrease in latent heat flux. Therefore, surface absorption of the excess of shortwave radiation is balanced by a considerable increase in sensible heat flux. All of this is consistent with a larger increase in maximum than in minimum temperatures, resulting in a positive DTR, also in concordance with the results presented by Expósito et al. (2015).

During the summer months, the decrease in cloud cover is lower than in winter and has a smoother behavior for the different latitudes. Thus, the changes in the shortwave radiation incident on the surface are also smaller and do not have such a strong relationship with elevation. The most relevant local effect is the decrease in soil moisture in this season, being more pronounced in the upper part of the northern slopes of the island. This is reflected in a further decrease in latent heat flow in that area, which is compensated by an increase in sensible heat flow. In fact, it is in that zone where the change in DTR is largest. Otherwise, the expected change of minimum and maximum temperatures follows the expected behavior in the study region, that is, an EDW. As the layers of the atmosphere at higher elevations will experience stronger warming in the future, the change in longwave incident radiation over the surface will increase, which is reflected in the rise in net radiation. At low elevations, the temperature increase will not be as large, so the upward longwave radiation will not change as much as the downward longwave radiation, causing a larger change in net radiation.

4.2. Return periods

Using the 20-year return level for the maximum temperature in the recent past (HIS), return periods in future projections were calculated. Due to the temperature increase predicted by the models, a reduction in the return period is to be expected. Thus, at mid-century, this parameter is, on average, between 4 and 5 years depending on the RCP used. Nevertheless, at the end of the period, this value drops to 3 years for the simulations driven by RCP4.5 and about 2 years for the RCP8.5 scenario. Due to the rapid temperature increase in the mountainous area predicted by the models compared to lowlands, it is observed how these areas, and in general, the western islands, are the most affected in the reduction of the return period for the maximum temperature. Table 5 indicates the return periods in years, for the WRF simulated projections

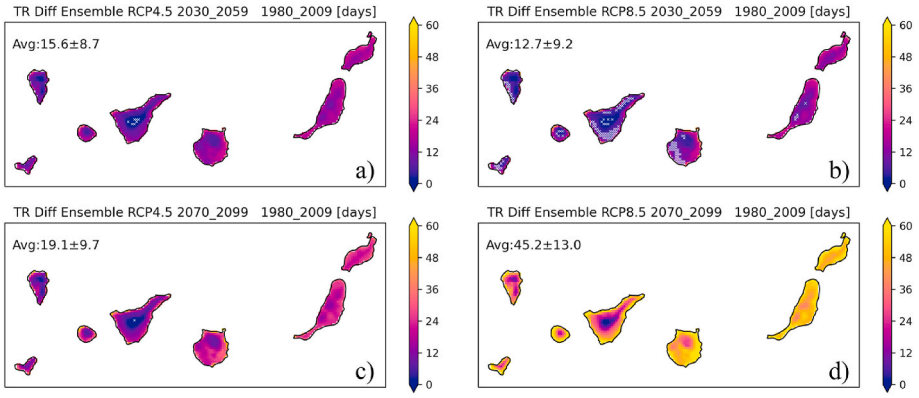

Fig. 11. As Fig. 9 but for the TR variable (days). White dots indicate pixels without statistical significance.

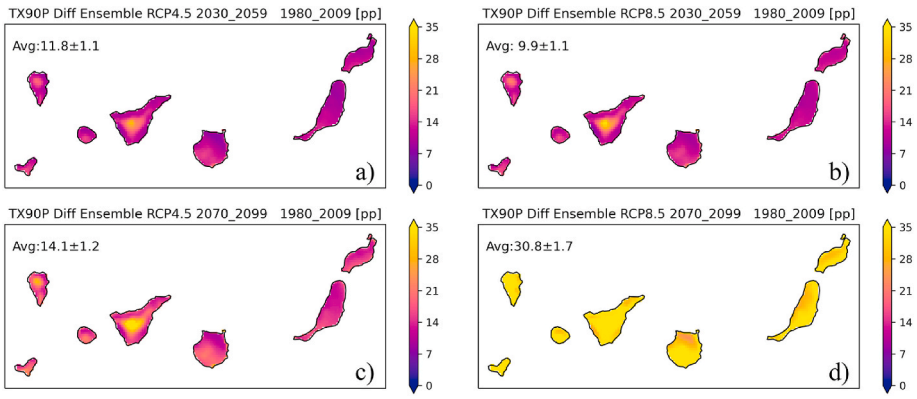

Fig. 12. Average differences in percentage points (pp) of days with Tx > 90th percentile obtained in the period 1980–2009, for the simulations of future projections (MID and END) corresponding to the RCP4.5 greenhouse emission scenarios (left column) and RCP8.5 (right column).

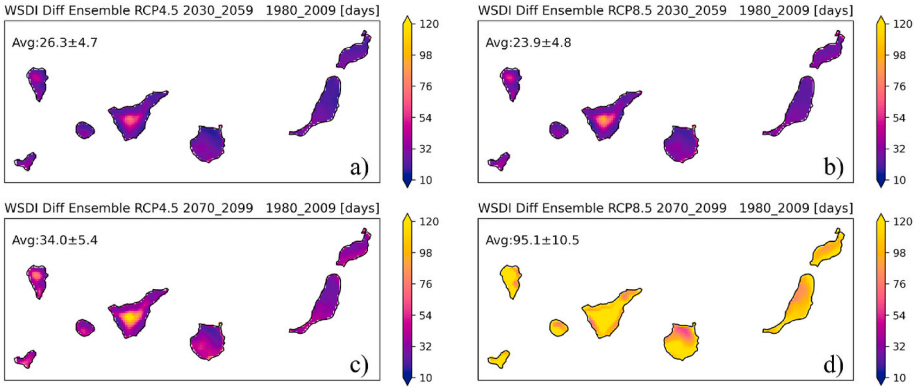

Fig. 13. The mean annual differences in the Warm-Spell Duration Index (days) for the simulations of future projections, i.e., the mean annual count of days, with at least 6 consecutive days, that exceed the 90th percentile of Tx obtained in the period 1980–2009.

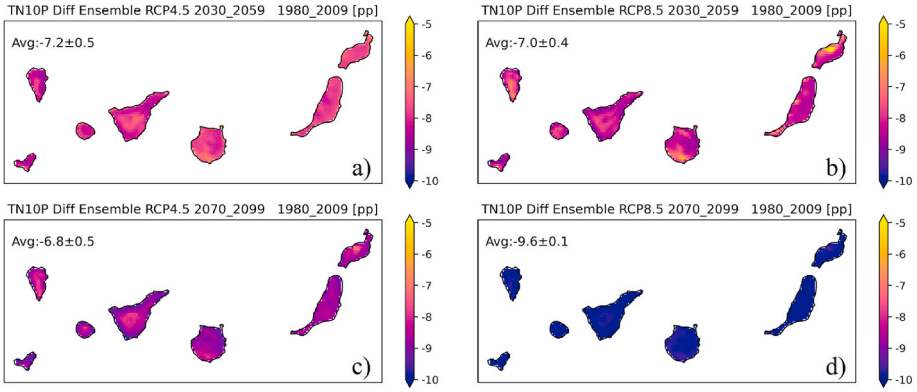

Fig. 14. As Fig. 12 but for the percentage points (pp) of days with Tn < 10th percentile obtained in the period 1980–2009.

on those land grid points nearest to the ECAD stations, whereas Fig. 16 shows the return period in years for the whole area.

5. Conclusions

In the current context of climate change, future temperature extreme events are one of the most serious problems humanity may have to face, not only environmentally but also social and economically. This study provides convection-permitting projections (3 km) of climatic temperature extremes focused on the Canary Islands. This information is central for the design of effective adaptation/mitigation strategies to the climate change effects in this archipelago. Previous studies that generated climate projections throughout this century in this region were based on the pseudo global warming strategy, making it difficult to study climate extremes. This work uses a dynamic downscaling methodology based on the WRF model, which was configured using as inputs (initial and boundary conditions) three CMIP5 models: GFDL-ESM2M, MIROC-ESM and IPSL-CM5. The climate projections were obtained for the time periods: 2030–2059 (MID) and 2070–2099 (END) and the RCPs 4.5 and 8.5 scenarios. The modeled reference period was 1980–2009 (HIS), for which future changes were calculated.

In a first step, the modeled indices using the ERA-Interim reanalysis data (1995–2004) as input in the WRF model and the ECAD observational data of nine stations were compared. The results show that the

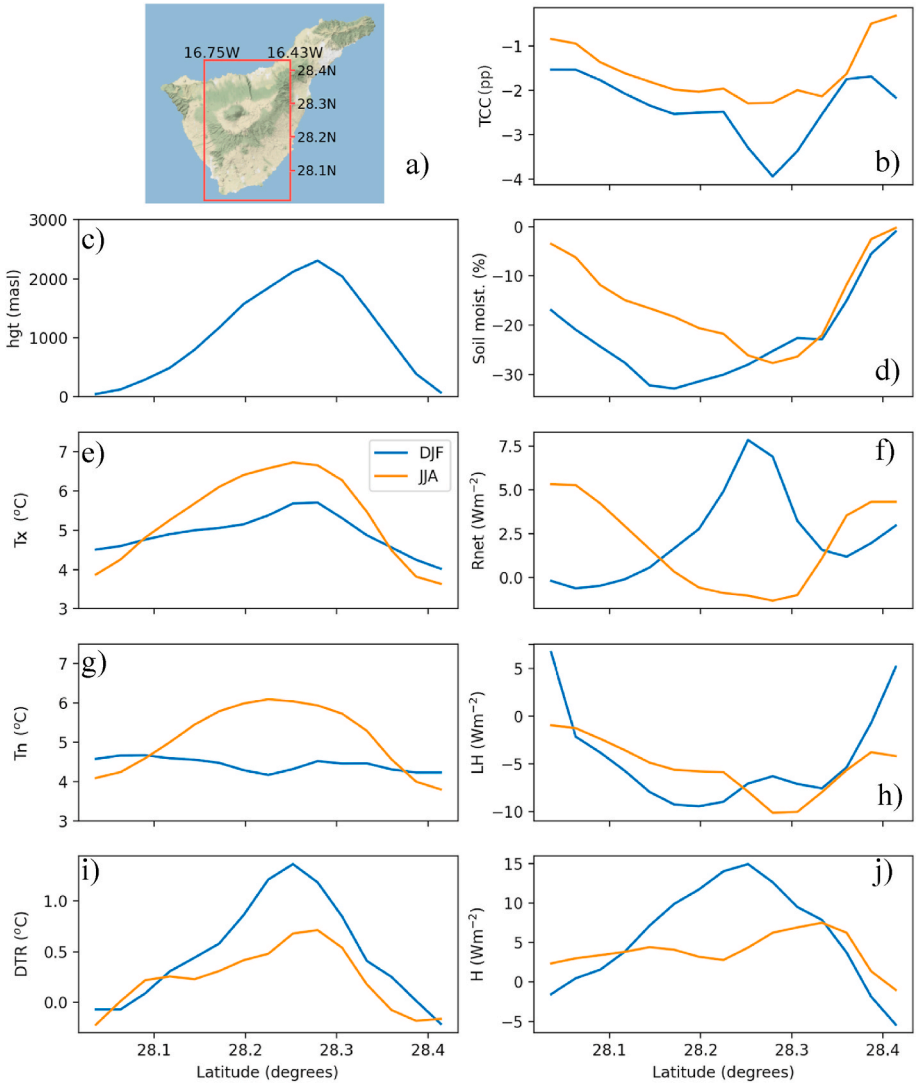

Fig. 15. Changes in the zonal average of several variables corresponding to the transect indicated in the map for the projected changes for END period and RCP8.5 pathway. Plots show seasonal means for winter (DJF) and summer (JJA), and correspond to MIROC-driven simulations. Hgt indicates terrain height (masl), Tx is daily maximum temperature (°C), Tn is daily minimum temperature (°C), DTR is diurnal temperature range (°C), TCC is total cloud cover (%), soil moist. is the percentage of change of the soil moisture, Rnet is the surface net radiation (Wm^{-2}), LH is the latent heat flux (Wm^{-2}) and H is the sensible heat flux (Wm^{-2}).

Table 5
Return periods in years for the simulations of the future projections in the model WRF nearest grid point to the ECAD stations. G indicates the GFDL model, I IPSL model and M is the MIROC model. Avg. is the average of the models. Finally, MID45 corresponds to the middle century period with RCP4.5, MID85 middle century with RCP8.5, END45, the end century period with RCP4.5 and END85 corresponds to the end century period with RCP8.5. The symbol "–" indicates bad data.

	IZO	TFN	ACE	FUE	VDE	SPC	SCT	TFS	LPA
G-MID45	3.5 ± 1.4	19 ± 14	4.5 ± 1.2	–	–	4.4 ± 1.7	–	–	–
I-MID45	1.3 ± 0.6	–	2.5 ± 0.7	–	3.3 ± 0.8	4.2 ± 1.0	–	6.0 ± 2.4	7.3 ± 3.7
M-MID45	1.2 ± 0.8	3.3 ± 1.7	3.6 ± 3.5	–	2.7 ± 0.7	2.8 ± 0.8	–	2.7 ± 1.2	3.1 ± 0.5
Avg.	1.5 ± 0.8	3.5 ± 2.4	3.0 ± 1.0	–	3.0 ± 0.8	3.5 ± 1.0	–	3.4 ± 1.5	3.2 ± 0.7
G-MID85	2.7 ± 1.2	4.9 ± 1.5	3.1 ± 0.6	8.6 ± 4.7	–	3.9 ± 1.5	6.1 ± 2.8	4.3 ± 1.8	4.3 ± 1.8
I-MID85	1.4 ± 0.1	4.7 ± 5.0	3.0 ± 1.0	–	2.8 ± 0.9	3.0 ± 0.7	–	7.1 ± 2.6	4.2 ± 2.0
M-MID85	1.9 ± 0.3	2.7 ± 1.0	3.1 ± 0.4	3.5 ± 1.0	2.3 ± 0.2	2.3 ± 0.3	–	3.2 ± 0.4	3.3 ± 0.6
Avg.	1.5 ± 0.2	3.4 ± 1.4	3.1 ± 0.5	3.7 ± 1.4	2.3 ± 0.3	2.5 ± 0.5	6.1 ± 2.8	3.3 ± 0.7	3.5 ± 0.9
G-END45	2.1 ± 0.9	3.0 ± 0.9	2.5 ± 0.4	3.4 ± 1.7	7 ± 1	3.0 ± 1.1	3.3 ± 1.1	3.8 ± 1.7	3.6 ± 1.3
I-END 45	1.0 ± 1.4	2.7 ± 0.9	2.3 ± 0.6	5.6 ± 2.3	2.1 ± 0.9	3.5 ± 0.9	2.8 ± 3.3	4.7 ± 1.1	4.3 ± 1.7
M-END45	–	1.5 ± 0.6	2.4 ± 1.0	–	1.4 ± 0.4	1.3 ± 0.1	2.9 ± 2.6	1.1 ± 0.7	3.6 ± 1.2
Avg.	1.8 ± 1.1	2.1 ± 0.8	2.4 ± 0.5	4.2 ± 1.9	1.5 ± 0.6	1.3 ± 0.2	3.2 ± 1.7	2.3 ± 1.0	3.7 ± 1.4
G-END85	–	1.4 ± 0.2	1.3 ± 0.3	1.8 ± 0.8	1.3 ± 0.8	–	1.5 ± 0.4	1.3 ± 0.4	1.1 ± 0.4
I-END85	–	1.7 ± 0.6	1.5 ± 0.3	–	1.6 ± 0.2	1.6 ± 0.3	1.4 ± 0.9	3.8 ± 1.1	2.8 ± 1.0
M-END85	–	–	–	2.3 ± 1.6	–	1.4 ± 0.4	–	–	2.4 ± 0.6
Avg.	–	1.4 ± 0.3	1.4 ± 0.3	1.9 ± 1.0	1.6 ± 0.3	1.5 ± 0.3	1.5 ± 0.5	1.6 ± 0.5	1.6 ± 0.5

WRF configuration introduces a bias, which is, on average, of −2.6 °C and −2.1 °C for TX and TN respectively. In addition, the indices obtained with the three CMIP5 input datasets and the ensemble at the ECAD stations were evaluated with those observed in the reference period. Biases are still observed between these values although it depends on the model, being the MIROC, in general, the results that best fit. However, concerning the range of variation of the modeled data, these properly reproduce those of the observed data, with mean skill

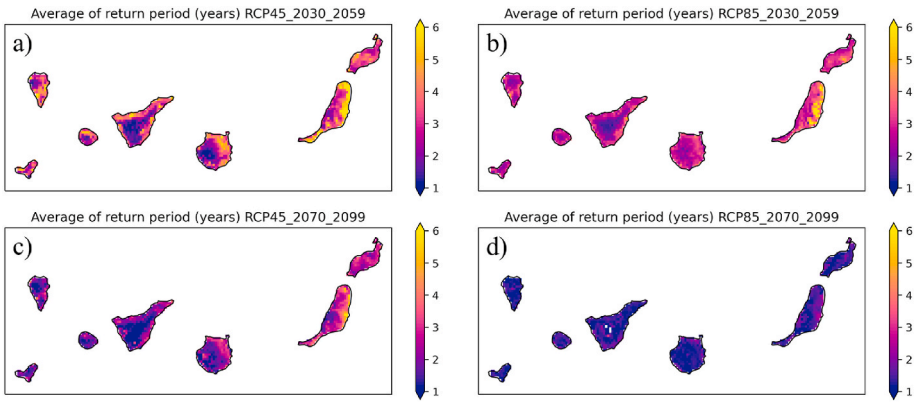

Fig. 16. Return periods in years for the 20-year return level of maximum temperature during the historical period using the simulations of the future projections (middle and end of the century) and corresponding to the greenhouse emission scenarios RCP4.5 (left column) and RCP 8.5 (right column). White dots indicate bad data.

scores for the ensemble PDF of the absolute indices about 0.85 ± 0.06, whereas for the threshold indices this value is 0.62 ± 0.27. The goodness of this comparison is also tested with the analysis of the Q-Q plots of the modeled versus the measured indices. For all the absolute indices the Q-Q plots show the data mainly localized along the straight-line y = x (ideal situation). However, the modeled variables based on thresholds, which use directly maximum or minimum daily absolute temperature values, generate worse results when compared with the observational ones.

Regarding the comparative of the return levels (maxima temperature) for a 20-year return period, estimated from GEV analysis, there is agreement between those obtained from the observations and those obtained from modeled data, since, on average considering all the stations except TFN and IZO (those at the highest altitude), their difference is less than 1.9 °C.

The changes between the future projections of the extreme temperature indexes and those for the recent past (HIS) show that in the middle of the century, no appreciable differences between simulations performed with either of the RCPs were found. An increase in extreme temperatures is observed in both simulations but this rise is similar in both realizations. However, as the input models follow the variations of the CO_2-equivalent concentrations, the simulations produce a greater increase in those for which the final forcing is 8.5 Wm^{-2} compared to those of 4.5 Wm^{-2}. In this most unfavorable scenario, the increase can be almost double for several extreme quantities such as TX or TN.

In general, as expected at the latitude at which the Canary Islands are located, simulated near-surface warming increases with elevation. However, the modulation of this general behavior at the local scale can only be explained by considering regional-scale processes involving the land surface and the orography. The main mechanisms that give rise to the observed temperature increase seem to be related to the decrease in total cloud cover (TCC) and soil moisture. This decrease in soil moisture has a direct effect on the decrease in latent heat flux and an increase in sensible heat flux, associated with a larger increase in maximum temperatures with respect to minimum temperatures. These changes depend on the orography and the orientation of the slopes.

Analyzing the statistically robust changes, with a 95% confidence interval, along the 21st century of these indices with respect to the HIS period, the following results can be summarized:

1 The TX and TN values increase both in the MID and END period and for both RCPs scenarios. The spatial average for the END period anticipates an increase in TX values of 2.0 ± 0.5 °C (RCP4.5) and 4.0 ± 0.5 °C (RCP8.5). And for TN is obtained 2.4 ± 0.4 (RCP4.5) and 4.4 ± 0.4 (RCP8.5). The DTR shows an increase close to 0.5 °C (about 1 °C at high altitude).
2 The TX90p shows an increase at the END period and for both scenarios. Changes in TX90p values reach, on average, 30 percentage points at the END period and RCP8.5. For the TN10p variable there is a decrease at the END period with a reduction about 10 percentage points considering the worst scenario.
3 The changes in WSDI show an increase in this index. The number of days for the WSDI index, at the END period and RCP8.5, increases between 40 and 180 days, with the major increase in high altitude zones. On the other hand, CSDI decreases with values that range between 2 and 10 days.
4 The return levels that in the HIS period were obtained with a return period of 20 years, will be obtained along the 21st century more frequently, with return periods between 1 and 6 years at the END period and RCP8.5.

In addition to the predicted global increase in mean temperature, there are possible local changes in the area of the Canary Islands that could affect the behavior of the temperature and should be studied. Among these, we highlight: a weakening of the thermal inversion layer, a change in the thermodynamic conditions in the marine boundary layer in the Atlantic Ocean, which could produce a change in the cloud regime in the Canary Islands region (Díaz et al., 2019); a notable decrease in cloud cover in the winter season (Pérez et al., 2019) and a decrease of wind speed during the summer season (González et al., 2017). The consequences of the adverse impacts of the increase in the temperature extremes should be analyzed for the conservation of the rich and sensible insular ecosystems. The economic and societal impacts of the increase in the extreme temperatures could be a problem of primary order in an insular region with high dependence on the goodness of its climate.

Author statement

Juan C Pérez: Conceptualization, resources, data curation, writing - reviewing and editing. Francisco J. Expósito: Conceptualization, methodology, validation, writing- original draft preparation and visualization. Albano González: Conceptualization, formal analysis, visualization, writing - reviewing and editing. Juan P. Díaz: Supervision.: Conceptualization, methodology, writing- original draft preparation and project administration and funding acquisition.

Declaration of competing interest

The authors declare that they have no known competing financial interests or personal relationships that could have appeared to influence the work reported in this paper.

Acknowledgments

We acknowledge the World Climate Research Programme's Working Group on Coupled Modelling, which is responsible for CMIP, and we thank the climate modeling groups (listed in Table 2 of this paper) for producing and making available their model output. For CMIP the U.S. Department of Energy's Program for Climate Model Diagnosis and Intercomparison provides coordinating support and led the development of software infrastructure in partnership with the Global Organization for Earth System Science Portals. This work was supported by projects CGL2015-67508-R, and RTC-2017-6409-3 funded by Ministerio de Ciencia e Innovación, Spain. The authors are grateful for the support of the PLANCLIMAC Project (MAC/3.5b/244). This Project is financed by the European Union INTERREG MAC 2014–2020 Program, co-funded by European Regional Development Fund (ERDF-FEDER). They also thank the Government of the Canary Islands, Consejería de Transición Ecológica, Lucha contra el Cambio Climático y Planificación Territorial, for their support (published agreement: B.O.C. No. 238, November 20, 2020). NOAA High Resolution SST data were provided by the NOAA/OAR/ESRL PSL, Boulder, Colorado, USA, from their Web site.

Appendix A. Supplementary data

Supplementary data to this article can be found online at https://doi.org/10.1016/j.wace.2022.100459.

References

AEMET, National Meteorological Agency, Spain, 2021. Climate Projections along the XXI Century. http://www.aemet.es/es/serviciosclimaticos/cambio_climat.

Atlas, Climate, 2012. Climate Atlas of the Archipelagos of the Canary Islands, Madeira and the Azores. The Meteorological State Agency of Spain and the Institute of Meteorology. Agencia Estatal de Meteorología, Ministerio de Agricultura, Alimentación y Medio Ambiente; Instituto de Meteorologia de Portugal, Lisboa. https://doi.org/10.31978/281-12-006-X.

Australian Bureau of Meteorology and CSIRO, 2014. Climate Variability, Extremes and Change in the Western Tropical Pacific: New Science and Updated Country Reports. Pacific-Australia Climate Change Science and Adaptation Planning Program Technical Report. Australian Bureau of Meteorology and Commonwealth Scientific and Industrial Research Organisation, Melbourne, Australia.

Bony, S., Colman, R., Kattsov, V.M., Allan, R.P., Bretherton, C.S., Dufresne, J., Hall, A., Hallegatte, S., Holland, M.M., Ingram, W., Randall, D.A., Soden, B.J., Tselioudis, G., Webb, M.J., 2006. How well do we understand and evaluate climate change feedback processes? J. Clim. 19 (15), 3445–3482. https://doi.org/10.1175/JCLI3819.1.

Chen, F., Dudhia, J., 2001. Coupling an advanced land surface-hydrology model with the Penn State-NCAR MM5 modeling system. Part II: preliminary model validation. Mon. Weather Rev. 129, 587–604. https://doi.org/10.1175/1520-0493(2001)129<0569:CAALSH>2.0.CO;2.

Coles, S., 2001. Classical extreme value theory and models, 45–73. In: An Introduction to Statistical Modeling of Extreme Values. Springer London. https://doi.org/10.1007/978-1-4471-3675-0_3, 2001.

Collins, W.D., Rasch, P.J., Boville, B.A., Hack, J.J., McCaa, J.R., Williamson, D.L., Briegleb, B.P., Bitz, C.M., Lin, S., Zhang, M., 2006. The formulation and atmospheric simulation of the community atmosphere model version 3 (CAM3). J. Clim. 19 (11), 2144–2161. https://doi.org/10.1175/JCLI3760.1.

Cooley, D., 2013. Return periods and return levels under climate change, 97–114. In: Extremes in a Changing Climate: Detection, Analysis and Uncertainty. Springer Netherlands. https://doi.org/10.1007/978-94-007-4479-0_4.

Di Luca, A., Pitman, A.J., de Elia, R., 2020a. Decomposing temperature extremes errors in CMIP5 and CMIP6 models. Geophys. Res. Lett. 47 https://doi.org/10.1029/2020GL088031.

Di Luca, A., de Elia, R., Bador, M., Argueso, D., 2020b. Contribution of mean climate to hot temperature extremes for present and future climates. Weather Clim. Extrem. 28 https://doi.org/10.1016/j.wace.2020.100255.

Díaz, J.P., Expósito, F.J., Pérez, J.C., González, A., Wang, Y., Haimberger, L., Wang, J., 2019. Long-term trends in marine boundary layer properties over the Atlantic Ocean. J. Clim. 32 (10), 2991–3004. https://doi.org/10.1175/JCLI-D-18-0219.1.

Dufresne, J.L., Foujols, M.A., Denvil, S., Caubel, A., Marti, O., Aumont, O., Balkanski, Y., Bekki, S., Bellenger, H., Benshila, R., Bony, S., Bopp, L., Braconnot, P., Brockmann, P., Cadule, P., Cheruy, F., Codron, F., Cozic, A., Cugnet, D., de Noblet, N., Duvel, J.P., Ethe, C., Fairhead, L., Fichefet, T., Flavoni, S., Friedlingstein, P., Grandpeix, J.Y., Guez, L., Guilyardi, E., Hauglustaine, D., Hourdin, F., Idelkadi, A., Ghattas, J., Joussaume, S., Kageyama, M., Krinner, G., Labetoulle, S., Lahellec, A., Lefebvre, M.P., Lefevre, F., Levy, C., Li, Z.X., Lloyd, J., Lott, F., Madec, G., Mancip, M., Marchand, M., Masson, S., Meurdesoif, Y., Mignot, J., Musat, I., Parouty, S., Polcher, J., Rio, C., Schulz, M., Swingedouw, D., Szopa, S., Talandier, C., Terray, P., Viovy, N., Vuichard, N., 2013. Climate change projections using the IPSL-CM5 Earth system model: from CMIP3 to CMIP5. Clim. Dynam. 40, 2123–2165. https://doi.org/10.1007/s00382-012-1636-1.

Dunne, J.P., John, J.G., Shevliakova, E., Stouffer, R.J., Krasting, J.P., Malyshev, S.L., Milly, P.C.D., Sentman, L.T., Adcroft, A.J., Cooke, W., Dunne, K.A., Griffies, S.M., Hallberg, R.W., Harrison, M.J., Levy, H., Wittenberg, A.T., Phillips, P.J., Zadeh, N., 2013. GFDL's ESM2 global coupled climate-carbon Earth system models. Part II: carbon system formulation and baseline simulation characteristics. J. Clim. 26, 2247–2267. https://doi.org/10.1175/JCLI-D-12-00150.1.

ECAD, 2021. European Climate Assessment and Dataset. https://www.ecad.eu.

Efron, B., Tibshirani, R.J., 1994. In: An Introduction to the Bootstrap, first ed. Chapman and Hall/CRC. https://doi.org/10.1201/9780429246593.

Expósito, F.J., González, A., Pérez, J.C., Díaz, J.P., Taima, D., 2015. High-resolution future projections of temperature and precipitation in the canary islands. J. Clim. 28, 7846–7856. https://doi.org/10.1175/JCLI-D-15-0030.1.

Freychet, N., Hegerl, G., Mitchell, D., et al., 2021. Future changes in the frequency of temperature extremes may be underestimated in tropical and subtropical regions. Commun Earth Environ 2, 28. https://doi.org/10.1038/s43247-021-00094-x, 2021.

González, A., Pérez, Juan C., Díaz, Juan P., Expósito, Francisco J., 2017. Future projections of wind resource in a mountainous archipelago, Canary Islands. Renew. Energy 104, 120–128. https://doi.org/10.1016/j.renene.2016.12.021.

Hartmann, D.L., Klein Tank, A.M.G., Rusticucci, M., Alexander, L.V., Bronnimann, S., Charabi, Y., Dentener, F.J., Dlugokencky, E.J., Easterling, D.R., Kaplan, A., Soden, B. J., Thorne, P.W., Wild, M., Zhai, P.M., 2013. Observations: atmosphere and surface. In: Stocker, T.F., Qin, D., Plattner, G.-K., Tignor, M., Allen, S.K., Boschung, J., Nauels, A., Xia, Y., Bex, V., Midgley, P.M. (Eds.), Climate Change 2013: the Physical Science Basis. Contribution of Working Group I to the Fifth Assessment Report of the Intergovernmental Panel on Climate Change. Cambridge University Press, Cambridge, United Kingdom and New York, NY, USA. https://doi.org/10.1017/CBO9781107415324.008.

Hong, S., Noh, Y., Dudhia, J., 2006. A new vertical diffusion package with an explicit treatment of entrainment processes. Mon. Weather Rev. 134, 2318–2341. https://doi.org/10.1175/MWR3199.1. American Meteorological Society.

Huang, B., Liu, C., Banzon, V., Freeman, E., Graham, G., Hankins, B., Smith, T., Zhang, H.-M., 2021. Improvements of the daily optimum interpolation sea surface temperature (DOISST) version 2.1. J. Clim. 34, 2923–2939. https://doi.org/10.1175/JCLI-D-20-0166.1 (V2.1).

IPBES, 2019. Summary for policymakers of the global assessment report on biodiversity and ecosystem services of the Intergovernmental Science-Policy Platform on Biodiversity and Ecosystem Services. Intergovernmental Science-Policy Platform on Biodiversity and Ecosystem Services (IPBES) Secretariat. https://doi.org/10.1111/padr.12283.

ISTAC, 2021. Statistical Institute of the Canary Islands. http://www.gobiernodecanarias.org/istac/.

Ito, R., Shiogama, H., Nakaegawa, T., Takayabu, I., 2020. Uncertainties in climate change projections covered by the ISIMIP and CORDEX model subsets from CMIP5. Geosci. Model Dev. (GMD) 13, 859–872. https://doi.org/10.5194/gmd-13-859-2020.

Ivanov, M., Warrach-Sagi, K., Wulfmeyer, V., 2018. Field significance of performance measures in the context of regional climate model evaluation. Part 1: temperature. Theor. Appl. Climatol. 132, 219–237. https://doi.org/10.1007/s00704-017-2100-2.

Kain, J.S., Fritsch, J.M., 1990. A one-dimensional entraining detraining plume model and its application in convective parameterization. J. Atmos. Sci. 47, 2784–2802. https://doi.org/10.1175/1520-0469(1990)047<2784:AODEPM>2.0.CO;2.

Kier, G., Kreft, H., Lee, T.M., Jetz, W., Ibisch, P.L., Nowicki, C., Mutke, J., Barthlott, W., 2009. A global assessment of endemism and species richness across island and mainland regions. Proc. Natl. Acad. Sci. U.S.A. 106, 9322–9327. https://doi.org/10.1073/pnas.0810306106.

Klein Tank, A.M.G., Wijngaard, J.B., Konnen, G.P., Bohm, R., Demaree, G., Gocheva, A., Mileta, M., Pashiardis, S., Hejkrlik, L., Kern-Hansen, C., Heino, R., Bessemoulin, P., Muller-Westermeier, G., Tzanakou, M., Szalai, S., Palsdottir, T., Fitzgerald, D., Rubin, S., Capaldo, M., Maugeri, M., Leitass, A., Bukantis, A., Aberfeld, R., Van Engelen, A.F.V., Forland, E., Mietus, M., Coelho, F., Mares, C., Razuvaev, V., Nieplova, E., Cegnar, T., Lopez, J.A., Dahlstrom, B., Moberg, A., Kirchhofer, W., Ceylan, A., Pachaliuk, O., Alexander, L.V., Petrovic, P., 2002. Daily dataset of 20th-century surface air temperature and precipitation series for the European Climate Assessment. Int. J. Climatol. 22, 1441–1453. https://doi.org/10.1002/JOC.773.

Klein Tank, A.M.G., Zwiers, F.W., Zhang, X., 2009. Guidelines on Analysis of Extremes in a Changing Climate in Support of Informed Decisions for Adaptation. Climate Data and Monitoring WCDMP-No. 72. WMO-TD. WMO, Technical Document 55. ISBN: 940074479X. [Available online at: http://www.wcrp-climate.org/documents/WCDMP_TD_1500.pdf.

Klok, E.J., Tank, A.M.G.K., 2009. Updated and extended European dataset of daily climate observations. Int. J. Climatol. 29, 1182–1191. https://doi.org/10.1002/JOC.1779.

Kotlarski, S., Bosshard, T., Lüthi, D., et al., 2012. Elevation gradients of European climate change in the regional climate model COSMO-CLM. Climatic Change 112, 189–215. https://doi.org/10.1007/s10584-011-0195-5.

Lim, K.S.S., Hong, S.Y., 2010. Development of an effective double-moment cloud microphysics scheme with prognostic cloud condensation nuclei (CCN) for weather and climate models. Mon. Weather Rev. 138, 1587–1612. https://doi.org/10.1175/2009MWR2968.1.

Meinshausen, M., Smith, S.J., Calvin, K., Daniel, J.S., Kainuma, M.L.T., Lamarque, J., Matsumoto, K., Montzka, S.A., Raper, S.C.B., Riahi, K., others, 2011. The RCP greenhouse gas concentrations and their extensions from 1765 to 2300. Climatic Change 109, 213–241. https://doi.org/10.1007/s10584-011-0156-z. Springer.

Minder, J.R., Letcher, T.W., Liu, C., 2018. The character and causes of elevation-dependent warming in high-resolution simulations of rocky mountain climate change. J. Clim. 31 (6), 2093–2113. https://doi.org/10.1175/JCLI-D-17-0321.1.

Mooney, C.Z., Duval, R.D., 1993. Bootstrapping. SAGE Publications, Inc. https://doi.org/10.4135/9781412983532.

Nurse, L.A., McLean, R.F., Agard, J., Briguglio, L.P., Duvat-Magnan, V., Pelesikoti, N., Tompkins, E., Webb, A., 2014. Small islands. In: Barros, V.R., Field, C.B., Dokken, D. J., Mastrandrea, M.D., Mach, K.J., Bilir, T.E., Chatterjee, M., Ebi, K.L., Estrada, Y.O., Genova, R.C., Girma, B., Kissel, E.S., Levy, A.N., MacCracken, S., Mastrandrea, P.R., White, L.L. (Eds.), Climate Change 2014: Impacts, Adaptation, and Vulnerability. Part B: Regional Aspects. Contribution of Working Group II to the Fifth Assessment Report of the Intergovernmental Panel on Climate Change. Cambridge University Press, Cambridge, United Kingdom and New York, NY, USA, pp. 1613–1654.

Pepin, N., Bradley, R.S., Diaz, H.F., et al., 2015. Elevation-dependent warming in mountain regions of the world. Nat. Clim. Change 5, 424–430. https://doi.org/10.1038/nclimate2563.

Pérez, J.C., Díaz, J.P., González, A., Expósito, F.J., Rivera-Lopez, F., Taima, D., 2014. Evaluation of WRF parameterizations for dynamical downscaling in the canary islands. J. Clim. 27, 5611–5631. https://doi.org/10.1175/JCLI-D-13-00458.1.

Pérez, Juan C., González, Albano, Díaz, Juan P., Expósito, Francisco J., Felipe, Jonatán, 2019. Climate change impact on future photovoltaic resource potential in an orographically complex archipelago, Canary Islands. Renew. Energy 133, 749–759. https://doi.org/10.1016/j.renene.2018.10.077.

Perkins, S.E., Pitman, A.J., Holbrook, N.J., McAneney, J., 2007. Evaluation of the AR4 climate models' simulated daily maximum temperature, minimum temperature, and precipitation over Australia using probability density functions. J. Clim. 20, 4356–4376. https://doi.org/10.1175/JCLI4253.1.

Petzold, J., Magnan, A.K., 2019. Climate change: thinking small islands beyond small island developing states (SIDS). Climatic Change 152, 145–165. https://doi.org/10.1007/s10584-018-2363-3.

Schulzweida, U., 2019. CDO User Guide. https://doi.org/10.5281/zenodo.3539275.

Sillmann, J., Kharin, V.V., Zhang, X., Zwiers, F.W., Bronaugh, D., 2013. Climate extremes indices in the CMIP5 multimodel ensemble: Part 1. Model evaluation in the present climate. J. Geophys. Res. Atmos. 118, 1716–1733. https://doi.org/10.1002/jgrd.50203.

Skamarock, W.C., Klemp, J.B., Dudhia, J., Gill, D.O., Barker, D.M., Duda, M.G., Huang, X.-Y., Wang, W., Powers, J.G., 2008. A Description of the Advanced Research WRF Version 3. NCAR Tech, p. 113. https://doi.org/10.5065/D68S4MVH. Note NCAR/TN-475+STR.

Skamarock, W.C., Klemp, J.B., Dudhia, J., Gill, D.O., Liu, Z., Berner, J., Wang, W., Powers, J.G., Duda, M.G., Barker, D.M., Huang, X., 2019. A Description of the Advanced Research WRF Model Version 4. NCAR Technical Notes. https://doi.org/10.5065/1dfh-6p97. NCAR/TN-556+STR.

Sperling, F.N., Washington, R., Whittaker, R.J., 2004. Future climate change of the subtropical North Atlantic: implications for the cloud forests of Tenerife. Climatic Change 65, 103–123. https://doi.org/10.1023/B:CLIM.0000037488.33377.bf.

Stegehuis, A.I., Teuling, A.J., Ciais, P., Vautard, R., Jung, M., 2013. Future European temperature change uncertainties reduced by using land heat flux observations. Geophys. Res. Lett. 40, 2242–2245. https://doi.org/10.1002/grl.50404.

Taylor, K.E., Stouffer, R.J., Meehl, G.A., 2012. An overview of CMIP5 and the experiment design. Bull. Am. Meteorol. Soc. 93, 485–498. https://doi.org/10.1175/BAMS-D-11-00094.1. American Meteorological Society.

van Vuuren, D.P., Edmonds, J., Kainuma, M., et al., 2011. The representative concentration pathways: an overview. Climatic Change 109, 5. https://doi.org/10.1007/s10584-011-0148-z, 2011.

Varotsos, K.V., Karali, A., Lemesios, G., et al., 2021. Near future climate change projections with implications for the agricultural sector of three major Mediterranean islands. Reg. Environ. Change 21, 16. https://doi.org/10.1007/s10113-020-01736-0.

Watanabe, S., Hajima, T., Sudo, K., Nagashima, T., Takemura, T., Okajima, H., Nozawa, T., Kawase, H., Abe, M., Yokohata, T., Ise, T., Sato, H., Kato, E., Takata, K., Emori, S., Kawamiya, M., 2011. MIROC-ESM 2010: model description and basic results of CMIP5-20c3m experiments. Geosci. Model Dev. (GMD) 4, 845–872. https://doi.org/10.5194/gmd-4-845-2011.

Whan, Kirien, Zscheischler, Jakob, Orth, Rene, Shongwe, Mxolisi, Rahimi, Mohammad, Asare, Ernest O., Seneviratne, Sonia I., 2015. Impact of soil moisture on extreme maximum temperatures in Europe, 2015 Weather Clim. Extrem. 9, 57–67. https://doi.org/10.1016/j.wace.2015.05.001. ISSN 2212-0947.

Wijngaard, J.B., Tank, A.M.G.K., Konnen, G.P., 2003. Homogeneity of 20th century European daily temperature and precipitation series. Int. J. Climatol. 23, 679–692. https://doi.org/10.1002/joc.906.

Zhang, X.B., Alexander, L., Hegerl, G.C., Jones, P., Tank, A.K., Peterson, T.C., Trewin, B., Zwiers, F.W., 2011. Indices for Monitoring Changes in Extremes Based on Daily Temperature and Precipitation Data, vol. 2. Wiley Interdisciplinary Reviews-Climate Change, pp. 851–870. https://doi.org/10.1002/wcc.147.